12th AIAA International Space Planes and Hypersonic Systems and Technologies,
Norfolk, Virginia 15 - 19 Dec 2003

Large Eddy Simulation of Scramjet Combustion Using a Subgrid Mixing/Combustion Model

F. Génin*, B. Chernyavsky†, S. Menon‡
School of Aerospace Engineering
Georgia Institute of Technology
Atlanta, Georgia 30332

1 Abstract

Simulations of a hydrogen-fueled scramjet with hydrogen jet injection at the base of a wedge in a co-flowing air free-stream are performed for both non-reacting and reacting cases using Large Eddy Simulation (LES). Since fuel-air mixing is fundamental for accurate prediction of heat release effects, a subgrid mixing and combustion model developed earlier for subsonic combustion is employed in this study. An unique advantage of this model is that it allows closure of the reaction kinetics in an exact manner and also allows inclusion of molecular diffusion effects within the subgrid. Both these issues are considered critical for modeling $H_2 - O_2$ mixing and combustion. Predictions using this model (called the Linear Eddy Mixing (LEM) model) are compared to experimental data from DLR, earlier Reynolds Averaged Navier-Stokes (RANS) predictions, and current LES with subgrid Eddy Break-Up (EBU) closure. The results show that in general, LES gives better agreement with data and in particular, the LES-LEM approach is able to better predict the temperature in the far field. These results suggest that the LES-LEM approach has the potential for providing an accurate means for predicting supersonic combustion.

2 Introduction

In recent years, the United States and the world aerospace community have shown a renewed interest in hypersonic flying vehicles. The current road-map of the aerospace technology development indicates several areas of application for hypersonic vehicles, *e.g.*, military, long range passenger transport ('*Orient Express*') and Reusable Launch Vehicle (RLV). An advanced Mach 5 passenger aircraft would be capable of decreasing the flight time from the continental United States to Europe (distance of 7,400 km) to 1.3 hours, to Japan (8,900 km) to 1.6 hours and to Australia (12,200 km) to 2.5 hours, or a factor of 2-5 in comparison with current values. Another area of hypersonic application is RLV, either in Single Stage To Orbit (SSTO) or Two Stage To Orbit (TSTO) configurations. Such RLV can decrease the price of launching payload to the Low Earth Orbit from current value of about $ 10,000/kg down to $ 1,000/kg, which is considered a necessary prerequisite for the successful commercial utilization of space and for the sustained exploration of the Solar System.

The successful development of such flying vehicles would depend, to a large extent, on the development of an efficient propulsion system. Turbojets, which are the most commonly used propulsion systems for subsonic and moderately supersonic aircraft, lose their advantage of efficiency and economy of operation at Mach numbers above M = 3. Rocket engines, successfully used to date in the space launcher systems, are unattractive as well (at least for endoatmospheric vehicle) due to their poor fuel economy and inherently lower safety. Therefore, the propulsion system of choice for flight in M = 3 to 5 regime is a ramjet and beyond that in the M = 5 to 15 regime is a ramjet with supersonic combustion (scramjet).

Achieving scramjet propulsion beyond Mach 8 is still an unsolved problem since fuel-air mixing and combustion in high Mach number stream is a major challenge. Experimental study beyond Mach 8 in ground facilities is also a major challenge and currently, only very limited run-time facilities are available. This makes experimental optimization of the scramjet engine design nearly impossible at high M regime. The more cost-efficient way of investigating the propulsion system performance at these flight regimes, therefore, lies in the use of sophisticated computer simulations, provided that the simulation models have the requisite accuracy. Over the last quarter of century, computational fluid dynamics (CFD) has gradually become a major research tool playing an extensive role in aerospace science development.[1] In addition to allowing to analyze flow conditions which can not be readily obtained otherwise, CFD can greatly reduce the length and cost of the design cycle, due to the continuous advances in computer technology and the development of more sophisticated flow simulation software.

A promising technique for predicting the effects of

*AIAA Student Member, Graduate Research Assistant
†AIAA Member, Postdoctoral Fellow
‡AIAA Associate Fellow, Professor

turbulence in flows of technological interest is Large Eddy Simulation (LES).[2,3] In LES, all scales larger than the grid is modeled using a space and time accurate scheme and only the small scales are modeled using a subgrid model that is considered relatively universal. The direct computation of the large, energy-containing eddies (which are geometry and flow dependent features) gives LES more generality than the RANS method, which models the entire spectrum of turbulent motions. The computational cost of LES, although significant is fast becoming reasonable with the advent of massivelly parallel computers.

Although application of LES to many subsonic non-reacting[4] and reacting[5,6,7] have been reported, application to supersonic and/or hypersonic flows has been limited so far. In particular, LES of scramjet flow field will require not only accurate simulation of the large-scale features determined by the engine design but also of the small-scale mixing process that dominates fuel-air mixing and combustion process. In addition, finite-rate kinetics has to be included properly in the simulation model. This is problematic in classical LES since all the small-scales are modeled, but for accurate prediction of combustion the small-scale features must be resolved. Past attempts at the chemical kinetics closure have been somewhat ad hoc with extension of RANS closures to LES, such as the subgrid Eddy Breakup (EBU) model[8] which is an extension of the RANS EBU model,[9] *etc.*).

In this paper, we report on the application of the LEM model as a subgrid closure for scalar mixing and combustion in supersonic flows. Earlier, this LES-LEM approach has been applied to many canonical and full-scale (e.g., gas turbine) reacting flows[10,11,12,13] with excellent success in predicting features that conventional LES or RANS could not. However, all past results were limited to subsonic flows. Here, we discuss the results of LES-LEM of supersonic non-reacting and reacting flows.

3 Governing Equations

3.1 LES Governing Equations

The governing equations for LES are obtained by applying a spatial filter (based on the grid size $\overline{\Delta}$) to the compressible Navier-Stokes equations for the mass, momentum and energy conservation. The use of Favre averaging is common in the study of compressible flow, and is defined by $\widetilde{f} = \overline{\rho f}/\overline{\rho}$, where the over-line stands for temporal averaging. The resulting conservative equations are given by:

$$\begin{cases} \frac{\partial \overline{\rho}}{\partial t} + \frac{\partial \overline{\rho}\widetilde{u_i}}{\partial x_i} = 0 \\ \frac{\partial \overline{\rho}\widetilde{u_i}}{\partial t} + \frac{\partial}{\partial x_i}\left[\overline{\rho}\widetilde{u_i}\widetilde{u_j} + \overline{p}\delta_{ij} - \overline{\tau_{ij}} + \tau_{ij}^{sgs}\right] = 0 \\ \frac{\partial \overline{\rho}\widetilde{E}}{\partial t} + \frac{\partial}{\partial x_i}\left[\left(\overline{\rho}\widetilde{E} + \overline{p}\right)\widetilde{u}_i + \overline{q_i} - \right. \\ \qquad \left. \widetilde{u}_j\overline{\tau_{ij}} + H_{ij}^{sgs} + \sigma_{ij}^{sgs}\right] = 0 \end{cases} \quad (1)$$

Perfect gas is assumed, with a constant specific heats ratio of 1.4. Both the viscosity and the thermal conductivity of the species were approximated by a Sutherland law. The mixture viscosity is computed as a function of the species mole fractions Ξ, following Wilke:[14]

$$\mu_{mix} = \sum_{i=1}^{n} \frac{\Xi_i \mu_i}{\sum_{j=1}^{n} \Xi_j \phi_{ij}} \quad (2)$$

$$where: \phi_{ij} = \frac{\left[1 + \left(\mu_i/\mu_j\right)^{1/2}\left(M_j/M_i\right)^{1/4}\right]^2}{\left(8 + 8M_i/M_j\right)^{1/2}} \quad (3)$$

A similar approach was used for the mixed thermal conductivity computation.

Several terms in the LES equations require closure. Here, a closure based on a transport model for the subgrid kinetic energy k^{sgs} is used to close the momentum and energy subgrid fluxes. In this approach, a one-equation model for k^{sgs}:

$$\frac{\partial \overline{\rho} k^{sgs}}{\partial t} + \frac{\partial}{\partial x_i}\left(\overline{\rho}\widetilde{u_i}k^{sgs}\right) = \quad (4)$$

$$P^{sgs} - D^{sgs} + \frac{\partial}{\partial x_i}\left(\frac{\overline{\rho}\nu_t}{Pr_t}\frac{\partial k^{sgs}}{\partial x_i}\right) \quad (5)$$

is solved along with the LES equations. Here, ν_t is the turbulent viscosity and Pr_t is the turbulent Prandtl number. P^{sgs} is the subgrid kinetic energy production which is given and D^{sgs} is the subgrid kinetic energy dissipation.

$$\nu_t = C_\nu \sqrt{k^{sgs}}\ \overline{\Delta} \quad (6)$$

$$P^{sgs} = -\tau_{ij}^{sgs}\frac{\partial \widetilde{u_i}}{\partial x_j} \quad (7)$$

$$D^{sgs} = C_\epsilon \overline{\rho}\frac{\sqrt{(k^{sgs})^3}}{\overline{\Delta}} \quad (8)$$

Given ν_T the subgrid stresses and energy flux are closed as follows:

$$\tau_{ij}^{sgs} = -2\overline{\rho}\nu_T\left(\widetilde{S_{ij}} - \frac{1}{3}\widetilde{S_{kk}}\delta_{ij}\right) + \frac{2}{3}\overline{\rho}k^{sgs}\delta_{ij} \quad (9)$$

$$H_i^{sgs} = -\overline{\rho}\frac{\nu_T}{Pr_t}\frac{\partial \widetilde{H}}{\partial x_i} \quad (10)$$

The subgrid viscous work , σ_i^{sgs}, that appears in the filtered energy equation, was neglected, based on the earlier work of Kim *et al.*[15] In the above closure, two model coefficients C_ν and C_ϵ appear. Currently, we employ constant values of 0.067 and 0.916 for these constants based on earlier evaluation of these parameters.[10] A localized dynamic approach has also been developed[5] to compute these coefficients as a part of the solution. This approach is currently being evaluated for supersonic combustion and will be reported later.[16] However, the current results are not expected to be drastically changed with the dynamic approach.

3.2 Linear Eddy Mixing Model

In the LEM model[17, 18, 19, 20] the various physical processes, such as large scale advection, small scale mixing, molecular diffusion and chemical reaction are resolved at their relevant length and time scales. This model is implemented as a subgrid model in the LES-LEM approach, as briefly summarized below.

In LES-LEM, the governing LES equations (noted above) are numerically integrated using a time and space accurate numerical scheme on an appropriate three-dimensional grid. No conservation equation for species are solved on the resolved LES grid.

The species/scalar field evolution is tracked using a **two-scale** numerical approach. In this technique, turbulent convection of the scalars is split into two parts: **large-scale advection** and **turbulent stirring** at the small (sub-grid) scales. Large scale advection is the convection that happens above the unresolved scales. This is modeled by using a Lagrangian scheme which explicitly transports mass across the finite-volume cell surfaces in a manner that is consistent with the mass transport in the Eulerian continuity equation solved on the resolved grid. Small-scale advection is the turbulent stirring by scales smaller than the resolved grid. Note that, turbulent convection at the sub-grid scales only transports fluid mass over sub-grids length scales and recovers the fine-scale mixing features that is absent in a conventional LES approach.

The scalar molecular diffusion, chemical reactions and heat release are all included within the LEM locally within each LES cell. To resolve all the scales of motion within the subgrid, these processes are resolved on a locally 1D grid. This idea relies on the following. (1) Small scale turbulence is locally homogeneous and isotropic, (2) Effect of heat-release and the associated thermal expansion on the flow is the same in all direction, and (3) The model in its basic form, has been shown[17] to capture the correct physics of scalar mixing at small-scales in homogeneous, isotropic turbulence.

The resolution within the LEM 1D domain is chosen to resolve all scales down to the Kolmogorov scale (if needed) and therefore, the subgrid reaction-diffusion process is considered exact locally. Thus, finite-rate kinetics can be included in exact form without requiring any closure (such as EBU) in LES-LEM. This ability is similar to the exact closure in scalar PDF models,[21] however, an unique feature of LES-LEM is that it also allows inclusion of molecular diffusion (including differential effects) in an exact manner. These two abilities of LES-LEM is considered important for predicting turbulent combustion, especially in a hydrogen-fueled system.

To describe this two-scale numerical method, consider the exact (i.e., unfiltered) evolution equation for a reactive scalar Φ, written in the Eulerian form:

$$\rho\frac{\partial\Phi}{\partial t}+\underbrace{\rho u_i\frac{\partial\Phi}{\partial x_i}}_{\text{C}}+\underbrace{\rho\frac{\partial}{\partial x_i}[-D_\Phi\frac{\partial\Phi}{\partial x_i}]}_{\text{D}}=\underbrace{\dot{w}_\Phi}_{\text{R}} \tag{11}$$

where the term C represents the total (large scale + small scale) convection, the term D represents the molecular diffusion and the term R represents the chemical reaction source term. Now, split $u_i = (\tilde{u_i} + u_i^{'})$ where, $\tilde{u_i}$ and $u_i^{'}$ are the contributions to the total convection from the resolved (large) and sub-grid (small) scales, repsectively. By grouping molecular diffusion and chemical reaction as small-scale processes one can split Eqn. [11] into two equations, one representing the three-dimensional large-scale processes and another representing the small-scale processes as follows.

$$\rho\frac{\Phi^*-\Phi}{\Delta t_{LES}}+\underbrace{\rho\tilde{u_i}\frac{\partial\Phi}{\partial x_i}}_{\text{L-C}}=0 \tag{12}$$

$$\rho\frac{\partial\Phi^*}{\partial t}+\underbrace{\rho u_i^{'}\frac{\partial\Phi^*}{\partial x_i}}_{\text{S-C}}+\rho\frac{\partial}{\partial x_i}[-D_\Phi\frac{\partial\Phi^*}{\partial x_i}]=\dot{w}_{\Phi^*} \tag{13}$$

Here, the term L-C represents large-scale convection and the term S-C represents the small-scale convection. Also, Δt_{LES} is the fluid-dynamic/acoustic (LES) time-step and Φ^* is the intermediate solution after the large-scale convection process. The large-scale advection processes (governed by Eqn. [12]) (which occurs in full 3D) and the small-scale advection (in Eqn. [13]) account for the complete evolution of the scalar fields.

3.3 Sub-grid LEM simulation

For the purpose of solving Eqn. [13], within each LES cell, a 1-D line segment known as the LEM domain is defined and discretized.

3.3.1 Molecular Diffusion and Chemical Reaction

The 1-D reaction-diffusion equation for the species and the temperature written in non-conservative form are solved numerically on the one-dimensional domain. These equations are given below.

$$\rho\frac{\partial Y_k}{\partial t}+F_{kstir}+\rho\frac{\partial}{\partial s}(-D_k\frac{\partial Y_k}{\partial s})=\dot{\omega}_k W_k \tag{14}$$

$$\rho c_p\frac{\partial T}{\partial t}+F_{Tstir}-\sum_{k=1}^{N}\rho c_{p,k}D_k(\frac{\partial Y_k}{\partial s})(\frac{\partial T}{\partial s})-\frac{\partial}{\partial s}(\bar{\kappa}\frac{\partial T}{\partial s})=-\sum_{k=1}^{N}h_k\dot{\omega}_k W_k \tag{15}$$

Here, T, $\bar{p}$ and ρ are the sub-grid temperature, the resolved pressure, and the sub-grid mass density, respectively. Y_k, W_k, $c_{p,k}$ and R_u, are the mass fraction, molecular weight, the specific heat at constant pressure, and the universal gas constant, respectively. Density in the sub-grid field is computed using the equation of state for the scalar mixture $\bar{p} = \rho T \sum_{k=1}^{N} Y_k R_u / W_k$ and the caloric relation is given by $h_k = \Delta h^o_{f,k} + \int_{T^o}^{T} c_{p,k}(T')dT'$. Also, $\dot{\omega}_k$, h_k, V_k and $\Delta h^o_{f,k}$ are respectively, the mass reaction rate, the enthalpy, the diffusion velocity and the standard heat of formation (at standard temperature, T^o) of the k-th species. Finally, $\bar{c}_p$, $\bar{\kappa}$ and D_k are respectively, the mixture averaged specific heat at constant pressure and the mixture thermal conductivity and the mixture averaged diffusivity of the k-th species.

In Eqns. [14] and [15], s denotes the co-ordinate direction on the 1-D domain. The orientation of the 1-D domain is usually aligned in the direction of the maximum scalar gradient.[18] The length of the 1-D domain is taken to be equal to that of the local LES filter width, Δ. Note that Eqns. [14] and [15] are equivalent to Eqn.[13] written in terms of sub-grid species and temperature field. Turbulent convection at the sub-grid scales of the form $u\partial Y_k/\partial s$ and $u\partial T/\partial s$ are symbolically represented as F_{kstir} and F_{Tstir}, respectively in Eqns. [14] and [15] and these are implemented explicitly, as discussed in the next section.

There are some assumptions inherent in the subgrid LEM approach, as currently implemented. These are noted below for completeness. However, as shown earlier, most if not all of these assumptions can be relaxed without violating the LES-LEM approach.

Assumptions

- Sub-grid pressure (inside the 1-D LEM domain) is assumed to be uniform and same as the resolved grid pressure. In the absence of strong pressure gradient such as those in shocks, and in highly compressible flows, it is reasonable to assume that the pressure in the sub-grid remains constant. However, pressure can vary spatially over the LES (resolved) grid. This assumption may eventually need to be re-assessed in supersonic flow if strong shocks or local compressibility effects have to be included. A method to deal with this effect has been developed and is currently under evaluation.

- The contribution from the sub-grid viscous work is neglected. Note that viscous work due to large-scale is still present in the 3D LES equations.

- Calorically perfect gas model assumed. However, it is straight-forward to extend LEM for thermally perfect model.

- Radiation effects are neglected in this study. However can be easily included in the model as shown elsewhere.[22]

3.3.2 Subgrid Turbulent Convection

The effects of the sub-grid velocity field on the sub-grid scalar fields are modeled (numerically) using stochastic re-arrangement events called *triplet maps*.[18] Each triplet map represents the action of an isotropic turbulent eddy on the sub-grid scalar field. The intuitive rationale for adopting the triplet map is illustrated in Fig. 1. Consider a mixing layer configuration shown in Fig. 1(a) with a plane material surface separating species A from species B. The bold straight line running from the top to the bottom shown in the box (dashed line) represents the initial concentration profile (uniform gradient). Horizontal lines (red and blue) represents the concentration isopleths at the initial time. Fig. 1(b) shows the distortion (stretching + compression) of the concentration isopleths due to the action of an eddy or vortex roll-up. The initial linear concentration profile evolves to a form qualitatively resembling the profile obtained by applying the triplet map to the linear profile. The scalar field produced is continuous and measure preserving (Note: scalar gradient field is not continuous).

Three parameters are needed to implement the turbulent stirring events: eddy size l, the eddy location within the 1D domain and the stirring frequency (mean event rate per unit length of the mapping domain) λ. The eddy size in the range Δ to η (Kolmogorov scale) is determined from an eddy size distribution $f(l)$, obtained using inertial range scaling in three-dimensional turbulence:[18]

$$f(l) = \frac{5}{3} \frac{l^{-8/3}}{(\eta^{-5/3} - \Delta^{-5/3})} \tag{16}$$

Here, η is determined from inertial range scaling law

$$\eta = N_\eta \frac{\Delta}{Re_\Delta^{3/4}} \tag{17}$$

where N_η is an empirical constant and Re_Δ is the sub-grid Reynolds' number based on the sub-grid turbulence intensity, kinematic viscosity and the local LES filter width, Δ. The constant N_η reduces the effective range of scales between Δ and η but does not change the turbulent diffusivity, as described in an earlier study.[23] The event location is randomly chosen from a uniform distribution and the event (mapping) rate (mean frequency per unit length) is[18]

$$\lambda = \frac{54}{5} \frac{\nu Re_\Delta}{C_\lambda \Delta^3} \frac{[(\Delta/\eta)^{5/3} - 1]}{[1 - (\eta/\Delta)^{4/3}]} \tag{18}$$

The time interval between events is then given as

$$\Delta t_{stir} = \frac{1}{\lambda \Delta} \tag{19}$$

where Δ is the length of the 1-D domain, which is also same as the local LES filter width. These mappings are implemented as a Poisson process in time. Note, that λ is not a function of length scale, l (of stirring) which implies that the interval between the stirring events are the same for all the length scales. Strictly speaking this is not true, but the following considerations justify this approach:

- The assumption of local isotropy in the sub-grid implies that the range of the stirring length scales are closely spaced in the wave-number space. This implies that their time-scale (or the turn-over time) is nearly same.
- The sub-grid Re_Δ and the filter width, Δ are varying spatially over the LES (resolved) grid. This implies that the the range of the stirring length scales and hence, the frequency of the stirring events also vary spatially over the LES (resolved) grid, even though it is same within the sub-grid.

The above formulation has two constants: C_λ and N_η, both of which arise from the use of scaling laws. In the earlier studies,[23,24] these parameters were defined by comparing LEM predictions to experimental data[25] in the flamelet regime. It is argued[26] that the scalar diffusivity due to triplet maps should equal the momentum diffusivity (by triplet maps), since inertial range eddies are responsible for both the processes. Therefore, the same value of the coefficient C_ν used in the expression for eddy viscosity expression (Eqn. [6]), should be used for scalar diffusivity C_λ. This value (0.067) was shown to be close to the values used in the earlier studies.[23,24] The present study, uses the same constant for all the simulations reported.

3.3.3 Volumetric Expansion

The final subgrid process in the LEM, which needs to be described is the volumetric expansion due to heat release. As mentioned earlier, constant pressure is assumed in the subgrid so that the heat release will cause volume expansion. Since the subgrid convection is modeled explicitly using triplet maps, volumetric expansion must be included explicitly as well. Volumetric gas expansion caused by heat release is modeled by expanding each linear-eddy cell in the subgrid domain by an amount equal to

$$\Delta V^*_{LEM,i} = \frac{\rho^n_i}{\rho^*_i} \tag{20}$$

where $\Delta V_{LEM,i}$ is the change in volume of LEM cell i. ρ^n_i and ρ^*_i are, respectively, the density of the "$i-th$" cell at the previous and the current time integration levels in the sub-grid simulation (not at the fluid-dynamic time-step, (Δt_{LES}) at LES level). In the previous studies,[27,28] the domain containing the expanded cells is re-gridded so that each cell is returned to its initial volume. In the present study, re-griding of the cells was done after the large-scale advection process, and not at this stage.

3.4 Hydrogen/Air Chemistry

3.4.1 Reaction Mechanism

In order to simulate the hydrogen-air combustion, a two-step mechanism, developed by Rogers and Chinitz[29] is used. In this mechanism, one intermediate species, OH, is taken into account, and the reaction steps are as described below:

$$H_2 + O_2 \rightleftharpoons 2OH \tag{21}$$

$$2OH + H_2 \rightleftharpoons 2H_2O \tag{22}$$

For these equilibrium reactions, an Arrhenius law is given by:

$$k_{f,i} = A_i(\phi) T^{N_i} exp(-\frac{E_i}{RT}) \tag{23}$$

where ϕ is the local equivalence ratio, R is the universal gas constant, and T the local temperature. The values of the coefficients in these equations are:

$$\begin{aligned} (1): A_1(\phi) &= \big(8.917\phi + \tfrac{31.433}{\phi} - 28.950\big)10^{47} \\ E_1 &= 4865 \\ N_1 &= -10 \end{aligned} \tag{24}$$

$$\begin{aligned} (2): A_2(\phi) &= \big(0.833\phi + \tfrac{1.333}{\phi} + 2.000\big)10^{64} \\ E_2 &= 42500 \\ N_2 &= -13 \end{aligned}$$

with A_i in $cm^3/(mol.s.K^{N_i})$, and E_i in cal/mol. Backward rates are computed using the equilibrium constants for these two reactions. This two-step mechanism was proven earlier[29] to be a good approximation for H_2/O_2 diffusion flames.

Note that since finite-rate kinetics can be included without requiring any closure in the LES-LEM approach any mechanism can be used and only the cost of the simulation is an issue. Speeding up the stiff chemistry evaluation remains a major issue in LES.

3.4.2 Reaction Rate Modeling

As noted above, in LES-LEM no explicit filtering of the reaction rate is needed and the exact rates can be included in the LEM domain. Therefore, any direct integration (DI) approach can be used to evolve the chemistry within the time step constraint for the diffusion equations 14, 15. Direct integration is very expensive but has been used successfully earlier.[30,31] To reduce the chemistry evaluation expense, *In situ* Adaptive Tabulation (ISAT)[32] method is also used here. With this approach, a speedup of O(6) has been observed so far and is consistent with earlier results.[33]

Further optimization is still required for LES-LEM application and is currently underway.

A conventional closure based on the subgrid EBU is also employed for comparison In this approach the filtered reaction rate is controlled by the turbulent timescales of the flow, corresponding to the subgrid scalar mixing rate. Reaction then occurs at the smallest of the time scale for mixing and consumption. The turbulent timescale was estimated by $\tau_{mix} = 0.2\overline{\Delta}/\sqrt{2k^{sgs}}$.

Since hydrogen-air combustion is considered very fast, past LES has employed infinite chemistry approach since it is very cost-effective. In this model, it is assumed that the chemical reaction occurs at infinite rate as soon as the reactants have mixed on a supergrid scale. Although results with this approach is also reported here, it must be noted that this method is inherently independent of the scalar mixing, and is thus not physical. The ignition time delay is not respected, and the predictions using this model is usually more qualitative than quantitative.

In addition to the three methods described above, comparison with a flamelet modeling approach adopted by Oevermann[34] is also reported here. In this study, the coupling between turbulence and reaction rate was handled by statistical description of the mixture fraction with a $\beta - PDF$ and a mean turbulent strain rate acting on the flame.

4 Numerical Methods

4.1 LES Numerical Implementation

The governing equations are solved using a finite-volume predictor-corrector scheme that is nominally second-order accurate in space and time. A fourth-order accurate scheme is also available but is not employed here. A Jameson type artificial dissipation[35] was added to the base scheme in order to extend the present scheme to deal with regions containing shocks.

Fully supersonic (Dirichlet) conditions are imposed at the inflow, and mixed subsonic/supersonic outflow is used: extrapolation is applied for supersonic outflow (Neumann Boundary Conditions), and non-reflecting characteristic outflow[36] for the subsonic regions. Impermeable, slip wall boundary conditions are used for the top and bottom walls, while no-slip conditions are enforced along the wedge. Periodic boundaries are set for the spanwise direction.

4.2 LEM Numerical Implementation

An operator split method[23,37] is used to integrate the stiff reaction-diffusion equations (Eqns. [14] and [15]). This splitting combines an explicit treatment of the LES resolved mass and momentum equations at the global time step with several explicit fractional steps for diffusion, reaction and turbulent stirring at the sub-grid scales. To solve the Eqns. [14] and [15] numerically, all spatial derivatives are discretized using a second-order accurate central difference schemes. A zero-gradient boundary condition is imposed for the species and for the temperature equation at subgrid domain boundaries.

A fixed number of LEM subgrid cells is used within every LES cell. The number of one-dimensional cells is estimated as follows. To represent an eddy using a triplet map, a minimum of 6 points are needed.[12] If the sub-grid Re_Δ is known, then using the expression $\eta = N_\eta \Delta Re_\Delta^{-3/4}$, an estimate of the smallest length scale can be obtained. Then, the maximum number of LEM cells needed to completely resolve all the sub-grid scales can be computed using the expression,

$$N_{max} = \min(\frac{\Delta_{ijk}}{\eta_{ijk}}) \tag{25}$$

where Δ_{ijk} and η_{ijk} are the local LES filter width and the Kolmogorov scale at the cell "ijk". The length of the linear eddy domain is set equal to the LES filter width Δ.

5 Results and Discussion

5.1 Test Problem

A representative scramjet flame holder experimentally studied at the Institute for Chemical Propulsion of German Aerospace Center (DLR)[38,39] is investigated in this study. This case has also been studied by Oeverman,[34] where both experimental date and numerical RANS results are compared. The configuration consists of a wedge in supersonic flow with hydrogen jet injected from a series of holes from the base of the wedge-shaped body. The combustion chamber is made of one-sided divergent channel with a base cross-section 40×50 mm. The supersonic free-stream flow is produced by a contoured Mach 2 Laval nozzle. Hydrogen is exhausted from the base of the wedge through 15 equally spaced nozzles, each with the diameter of 1 mm. The geometry of the case and relevant dimensions are shown in the Fig. 2 and the initial conditions are described in the Table 1. The turbulence level was 0.5% for the air stream and 5% for hydrogen stream.

For the numerical simulations, a section containing one nozzle at the center and two halves on each side of it were used for the hydrogen stream. This configuration is represented on Fig. 3, where Mach number isosurface is shown on top of a Z-vorticity plot. Periodic boundary in z direction is utilized.

A $250x121x25$ grid is used for the baseline calculations using a multi-block grid. Grid is clustered in the wake region and in the shear layer region to resolve the mixing region. For LES-LEM, 12 LEM cells are used in the LES cells in the region downstream of the base of the wedge.

The code is highly optimized for parallel simulation using MPI. The LES-LEM approach is naturally optimal in parallel machines and causes only a 10 percent

increase in overhead when compared to the baseline LES code. However, this cost is a function of the number of LEM cells employed and can increase if more LEM cells are used. Inclusion of finite-rate kinetics has a substantial impact on the overall cost and past studies have shown that overall cost can increase by a factor of seven[40] if DI (using standard stiff integrator is employed). However, using ISAT this cost can be brought down significantly.

All simulations are conducted on a Pentium III Xeon PC cluster using 32 CPUs. Simulations require around 830 single processor hours for the non-reacting case and around 7500 single processor hours for the reacting case using DI for one flow-through time. The reacting cost is decreased by a factor of around 3-4 when using ISAT. Typically, 2-3 flow through time data is used for statistical analysis. However, it is noted that due to time constraints and problems with the cluster, the LES-LEM cases have not evolved as long as the EBU and infinite-rate LES simulations. Therefore, the statistical quantities for these simulations are not fully settled down to the stationary state values. Nevertheless, the current comparison are considered representative of the various methods used here.

Finally, note that all the experimental data are extracted from the paper by Oevermann since the original experimental paper is no longer available. Therefore, comparison is only possible at locations for which data is shown in the above noted paper. Furthermore, other than temperature no data on the scalar field is reported in the experiments and in the RANS calculations. Thus, no comparison for the scalar field is possible.

Table 1 Inflow conditions for the air stream and the hydrogen jet

	Air	Hydrogen
M_a	2.0	1.0
$u^*[\frac{m}{s}]$	730	1200
$T^*[K]$	340	250
$p^*[10^5 Pa]$	1	1
$\rho^*[\frac{kg}{m^3}]$	1.002	0.097
Y_{O_2}	0.232	0
Y_{N_2}	0.736	0
Y_{H_2O}	0.032	0
Y_{H_2}	0	1

5.2 Non-Reacting Case

For the non-reacting studies, we simulate hydrogen-air mixing exactly as done in the experiments. Two LES have been performed: a conventional LES where the two species are modeled along with the LES equations and a gradient subgrid eddy diffusivity closure, and a LES-LEM approach in which scalar mixing is modeled within the LEM. Since only mean flow velocity data is available from the experiments, direct comparison of the scalar mixing cannot be performed. Thus, the effect of subgrid LEM approach is subtle in its indirect impact on the momentum mixing.

An oblique shock is formed at the tip of the wedge and an expansion fan occurs at the base of the wedge. Comparison and estimate of the oblique shock angle shows very good agreement with data. The boundary layer on the wedge surface separates at the base and a shear layer is formed. The hydrogen is injected at the base expands and mixes with the air in the shear layer. The initial wedge oblique shock reflects off the walls of the tunnel and interacts with the shear layer downstream of the initial mixing region. This results in a bending of the shear layer. After some distance, the wake is accelerated to supersonic speed, and the subsequent shock (reflecting from the walls) then pass through it. All these features can be seen on an average density contour plot, shown on Fig. 5. Overall, there is good agreement with experimental observation as can be seen in comparison with the shadowgraph image from the experiments, Fig. 4.

Laser Doppler Velocimetry (LDV) measurements of the flow have been taken at several locations in the experiments, and comparisons with the present simulations and with the earlier RANS calculation of Oevermann[34] are shown on Fig. 6 and 7.

The mean velocity profiles are correctly simulated both in the RANS simulation and in the present study, although a closer view shows substantial differences in predictions. At $x = 58$ mm downstream of the base, the mean velocity defect is captured quite accurately by the LEM-LES but is overpredicted by RANS and underpredicted by the conventional LES. All cases show deviation from measurements at the edges of the wake region. This descrepancy may be related to local intermittency effect that is not properly captured in the models. Further downstream at $x = 90$ mm the wake is recovering and the defect is smaller. All models predict similar results. All results (and data) show lack of symmetry in the wake profile and the deviation from measurements appears more on the lower side. The LES-LEM show reasonable agreement on the top side but underpredicts the measurements on the lower side. It is not clear if this is related to the lack of statistical stationarity of the computed flow. Simulation is still underway to address this concern.

The mean axial velocity fluctuation profile also show general agreement with experiments at the first station (at $x = 115$ mm, which is far downstream than the locations were the mean velocity data is reported above), as it can be seen on Fig. 7a. It can be seen that LES-LEM prediction is substantially better than the other two methods in the center part of the wake. The above noted lack of sufficient flow-through time in the LES-LEM is apparent in this figure (high frequency fluctuation in the curve) since typically, higher order moments take longer to settle down. Nevertheless, the

peak is well captured by LES-LEM whereas, conventional LES and RANS over predict this value. Further down stream the deviation form data is more apparent for all the simulated cases. The over prediction by RANS and LES is true since these solutions have settled down. It remain to be seen if the LES-LEM is also unable to capture the far field turbulent features, since more data needs to be used for averaging.

It is worth re-emphasizing that the LES-LEM effects on the velocity field is indirect since the LEM model only accounts for the scalar mixing. However, the resulting mixed region will impact the overall wake thickness and this in turn will modify the momentum mixing due to the non-linear nature of the flow.

To look at this issue further, the mean (i.e., LES-resolved) H_2 molar fraction distribution at two stations (where the mean velocity profiles are shown in Fig. 6) are shown in Fig. 8. In the conventional LES gradient diffusion is used for scalar subgrid flux and this results in an increased mass diffusion of the species in the transverse direction. Thus, the scalar width in the wake is increased for the conventional LES. On the other hand, in the LES-LEM approach, scalar transport on the LES grid is modeled using the Lagrangian transport approach for the LEM (described earlier) and this approach does not require (nor does it enforce) gradient diffusion. Thus, the scalar width is less in the LES-LEM case.

In summary, there is overall good agreement with measured data for both the LES studies performed here. Closer examination seem to suggest that the LES-LEM approach is obtaining a better agreement with data. This may be due to the subtle effect of how the scalar width is resolved in the LES-LEM. Some fluctuation features in the LES-LEM profiles is attributed to the lack of sufficient data in the statistical analysis. The current simulation is being continued to address this issue.

There are also some other uncertainty in the current simulations, The resolution adopted for this study does not resolve the wind tunnel walls with great accuracy. The boundary layers on the tunnel walls may influence the shock-boundary layer interactions which in turn can effect the far field of the wake where most of the measurements were made. Since there is no information on the inflow boundary layer and/or the tunnel wall boundary layers, these issues cannot be addressed.

5.3 Reacting Case

Reacting cases are simulated using the three approaches described in 3.4.2. A density contour plot of the simulated flow-field is shown in Fig. 10, and can be compared to the experimental Shadowgraph picture, Fig. 9. It is be seen that the growth of the wake resulting from the volumetric expansion due to the reaction is not reproduced with great accuracy. The shock/shear layer interaction however is well simulated: the impinging shock bends the shear layer, and the consequent flow direction matches the experimental behavior.

The mean velocity profile at two different stations ($x = 58$ mm and $x = 140$ mm) are shown in Figs. 11a and b. A good agreement is seen at the first station for all the simulations. The 3-D calculations show a reasonable trend in accordance with experimental data at the second station, while the 2D RANS calculation actually found a profile opposite to the experiments. An acceleration of the flow behind the wedge to supersonic speed, followed by a normal shock that reduced that region back to subsonic speeds was predicted in the earlier RANS calculation. However, this feature was absent in the experiments and also in the current 3D LES studies.

Turbulent statistics for the reacting case are presented in Fig. 12. Again, only the axial velocity fluctuation data is available for comparison. Good agreement is observed between the present LES studies and the experimental data. The amplitude and the width are found within a reasonable accuracy, and the defect that is observed at the centerline is also present in the present simulations. Further downstream, at $x = 90$ mm, all methods, except LES-LEM overpredict the velocity fluctuation.

Experimental and computed mean temperature profiles at three different stations are shown in Fig. 13. As was expected, the infinite chemistry approach is not satisfactory. Scalar mixing does not occur, and the flame doesn't penetrate the wake behind the wedge. This results in a double-spike configuration, whose amplitudes are excessively large compared to experimental values.

The EBU approach gives a better simulation of the heat release effect. It does not overshoot the experimental values, and in fact, tends to undershoot them. Very close to the base of the wedge the EBU profile shows very good agreement with experimental data. It clearly appears that this method of comparing mixing time to reaction time gives a far better approximation of the reaction process than infinite chemistry. However, as a result of the poor scalar mixing even in this method, it can be seen that the two flame fronts issued from the wedge base corners do not collapse as the experiments describe. As a result, further downstream, a double reaction zone still appears in the LES-EBU case.

The subgrid scalar mixing achieved by the LEM approach, on the other hand, shows an improved simulation of the heat release effect at the second and third stations. The chemical species are efficiently mixed, and the flame fronts, though underestimated at the first station do penetrate the wake/shear layer created by the wedge, and collapse to form a single flame front, as observed in the experiments. The RANS simulation of Oevermann[34] did capture the collapse of the flame

fronts, but overestimated the merging point, resulting in a wider hot zone, and a lower temperature. At the third station, both RANS and LEM approaches give a good estimate of the maximum temperature in the reacting region, but tend to spread the flame brush width. As noted earlier, the oscillations observed in the temperature profiles in the LES-LEM might be due to a too short averaging time for this set of data. Extending this average would probably give more accurate results.

6 Concluding remarks

In the present study, a numerical simulation of a scramjet was conducted using LES-LEM approach which incorporates subgrid mixing and combustion within the LES approach. The advantage of LES-LEM is that it can account for finite-rate kinetics without requiring closure and also includes the effect of molecular diffusion within the LEM. Both features are considered necessary for accurate prediction of turbulent combustion, especially for hydrogen-air mechanism. The present study extends the LES-LEM approach developed and validated earlier for subsonic reacting flows to supersonic mixing and combustion. The prediction by LES-LEM demonstrates good agreement with experimental data, especially when compared to RANS and EBU approaches. More accuracy could be gained in this study by extending the calorically perfect gas assumption to thermally perfect gas, first, and by implementing an efficient shock capturing method to the base scheme. Also, in order to capture to the full features of the flow, boundary layers on the top and bottom walls many also have to be properly resolved.

Acknowledgment

This work is supported by NASA under the URETI Center for Future Space Transport at University of Florida.

References

[1] Rupert, P., "The impact of supercomputers on CFD," *Computer Systems in Engineering*, Vol. 1, No. 6, 1990, pp. 1–6.

[2] Rogallo, R. S. and Moin, P., "Numerical Simulation of Turbulent Flows," *Annual Review of Fluid Mechanics*, Vol. 66, 1984, pp. 99–137.

[3] Lesieur, M., "Recent Developments in LES of Turbulence," *New Tools in Turbulence ModeLling*, edited by O. Metais and J. Ferziger, Springer-Les Editions De Physique, 1996, p. 222.

[4] Nelson, C. C., *Simulations of spatially evolving compressible turbulence using a local dynamic subgrid model*, Ph.D. thesis, Georgia Institute of Technology, Atlanta, GA, December 1997.

[5] Kim, W.-W. and Menon, S., "A New Incompressible Solver for Large-Eddy Simulations," *International Journal of Numerical Fluid Mechanics*, Vol. 31, 1999, pp. 983–1017.

[6] Kim, W.-W. and Menon, S., "Numerical Modeling of Turbulent Premixed Flames in the Thin-Reaction-Zones Regime," *Combustion Science and Technology*, Vol. 160, 2000, pp. 119–150.

[7] Fureby, C., "Large-Eddy Simulation of Combustion Instabilities in a Jet Engine Afterburner Model," *Combustion Science and Technology*, Vol. 161, 2000, pp. 213–243.

[8] Fureby, C. and Löfström, C., "Large-Eddy Simulations of Bluff Body Stabilized Flames," *Proceedings of the Combustion Institute*, Vol. 27, 1994, pp. 1257–1264.

[9] Spalding, D. B., "Mixing and Chemical Reaction in Steady Confined Turbulent Flames," *Thirteenth Symposium (International) on Combustion*, 1971, pp. 649–657.

[10] Chakravarthy, V. and Menon, S., "Large-Eddy Simulations of Turbulent Premixed Flames in the Flamelet Regime," *Combustion Science and Technology*, Vol. 162, 2001, pp. 175–222.

[11] Chakravarthy, V. and Menon, S., "Linear-Eddy Simulations of Reynolds and Schmidt Number Dependencies in Turbulent Scalar Mixing," *Physics of Fluids*, Vol. 13, 2001, pp. 488–499.

[12] Menon, S. and Calhoon, W., "Subgrid Mixing and Molecular Transport Modeling for Large-Eddy Simulations of Turbulent Reacting Flows," *Proceedings of the Combustion Institute*, Vol. 26, 1996, pp. 59–66.

[13] Sankaran, V., Porumbel, I., and Menon, S., "Large-Eddy Simulation of a Single-Cup Gas-Turbine Combustor," *AIAA-2003-5083, 39th AIAA Joint Propulsion Conference*, 2003.

[14] Wilke, C. R., "A Viscosity Equation for Gas Mixtures," *J. Chem. Phys.*, Vol. 18, 1950, pp. 517–519.

[15] Kim, W.-W., Menon, S., and Mongia, H. C., "Large Eddy Simulations of a Gas Turbine Combustor Flow," *Combustion Science and Technology*, Vol. 143, 1999, pp. 25–62.

[16] Sankaran, V. and Menon, S., "LES of Scalar mixing in supersonic mixing layers," *Submitted to : Proceedings of the Combustion Institute*, Vol. 30, 2004.

[17] Kerstein, A. R., "Linear-Eddy Model of Turbulent Scalar Transport and Mixing," *Combustion Science and Technology*, Vol. 60, 1988, pp. 391–421.

[18] Kerstein, A. R., "Linear-Eddy Model of Turbulent Transport II," *Combustion and Flame*, Vol. 75, 1989, pp. 397–413.

[19] Kerstein, A. R., "Linear-Eddy Modeling of Turbulent Transport. Part 6. Microstructure of Diffusive Scalar Mixing Fields," *Journal of Fluid Mechanics*, Vol. 231, 1991, pp. 361–394.

[20] Kerstein, A. R., "Linear-Eddy Modeling of Turbulent Transport. Part V: Geometry of Scalar Interfaces," *Physics of Fluids A*, Vol. 3, No. 5, 1991, pp. 1110–1114.

[21] Pope, S. B., "Turbulent Flame propagation in partially premixed flames," *Proceedings of the Summer Program, Center for Turbulence Research*, 1996.

[22] Zimberg, M. H., Frankel, S. H., Gore, J. P., and Sivathanu, Y. R., "A Study of Coupled Turbulent Mixing, Soot Chemistry and Radiation Effects Using the Linear Eddy Model," *Combustion and Flame*, Vol. 113, 1998, pp. 454–469.

[23] Smith, T. and Menon, S., "One-Dimensional Simulations of Freely Propagating Turbulent Premixed Flames," *Combustion Science and Technology*, Vol. 128, 1996, pp. 99–130.

[24] Smith, T. M. and Menon, S., "Model Simulations of Freely Propagating Turbulent Premixed Flames," *Proceedings of the Combustion Institute*, Vol. 26, 1996, pp. 299–306.

[25] Abdel-Gayed, R. G., Al-Khishali, K. J., and Bradley, D., "Turbulent Burning Velocities and Flame Straining in Explosions," *Proceedings of the Royal Society London A*, Vol. 39, 1984, pp. 393–414.

[26] Chakravarthy, V. and Menon, S., "Subgrid Modeling of Premixed Flames in the Flamelet Regime," *Flow, Turbulence and Combustion*, 2001.

[27] Smith, T., *Unsteady Simulations of Turbulent Premixed reacting flows*, Ph.D. thesis, Georgia Institute of Technology, Atlanta, GA, March 1998.

[28] Chakravarthy, V., *Stochastic Subgrid Modeling of Turbulent Premixed Flames*, Ph.D. thesis, Georgia Institute of Technology, Atlanta, GA, March 2000.

[29] Rogers, R. C. and Chinitz, W., "On the Use of Hydrogen-air Combustion Model in the Calculation of Turbulent Reacting Flows," *AIAA 82-0112*, 1981.

[30] Kerstein, A. R., "Linear-Eddy Modeling of Turbulent Transport. Part 4. Structure of Diffusion-Flames," *Combustion Science and Technology*, Vol. 81, 1992, pp. 75–86.

[31] Sankaran, V. and Menon, S., "Sub-grid Combustion Modeling for the Next Generation National Combustor Code," *NASA Report 2003*, 2003.

[32] Pope, S., "Computationally Efficient implementation of combustion chemistry using in situ adaptive tabulation," *Combustion Theory Modelling*, Vol. 1, 1997, pp. 41–63.

[33] Embouazza, M., Haworth, D. C., and Darabiha, N., "Implementation of Detailed Chemical Mechanisms into Multidimensional CFD Using *insitu* Adaptive Tabulation: Application to HCCI Engines," *SAE - 2002-01-2773*, 2002.

[34] Oevermann, M., "Numerical Investigation of Turbulent Combustion in a SCRAMJET Using Flamelet Modeling," *Aerospace Science and Technology*, Vol. 4, 2000, pp. 463–480.

[35] Jameson, A. and Baker, T. J., "Solution fo the Euler Equations for Complex Configurations," *AIAA 83-1929*, 1983.

[36] Poinsot, T. and Lele, S., "Boundary Conditions for Direct Simulations of Compressible Viscous Flow," *Journal of Computational Physics*, Vol. 101, 1992, pp. 104–129.

[37] Calhoon, W. H., Menon, S., and Goldin, G., "Comparison of Reduced and Full Chemical Mechanisms for Nonpremixed Turbulent H2-Air Jet Flames," *Combustion Science and Technology*, Vol. 104, 1995, pp. 115–141.

[38] Guerra, R., Waidmann, W., and Laible, C., "An Experimental Investigation of the Combustion of a Hydrogen Jet Injected Parallel in a Supersonic Air Stream," *AIAA 3^{r}d International Aerospace Conference*, 1991.

[39] Waidmann, W., Alff, F., Böhm, M., Brummund, U., Clauß, W., and Oschwald, M., "Supersonic Combustion of Hydrogen/Air in a Scramjet Combustion Chamber," *Space Technology*, Vol. 15, No. 6, 1995, pp. 421–429.

[40] Eggenspieler, G. and Menon, S., "Modeling of Pollutant Formation Near Lean Blow-Out in Gas Turbine Engines," *Direct and Large Eddy Simulation-5*, edited by R. Friedrich, B. J. Geurts, and O. Metais, Kluwer Press, Munich, 2003, 2003, p. to be published.

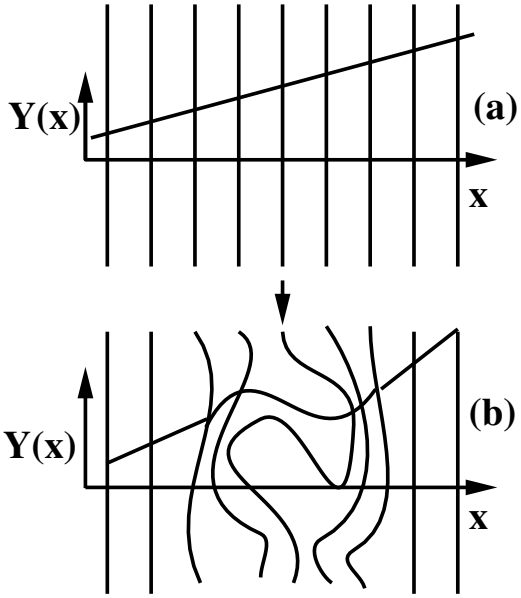

Fig. 1 triplet mapping approach

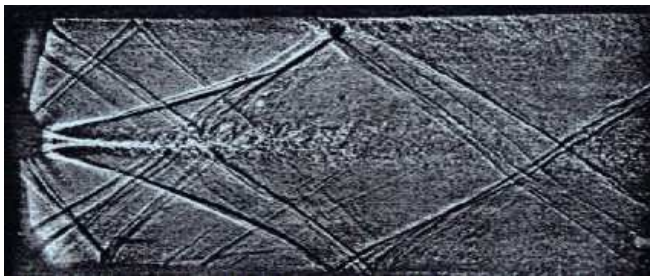

Fig. 4 Shadowgraph of the experimental flow-field

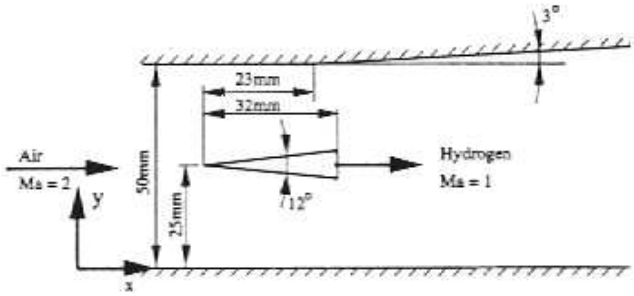

Fig. 2 Experimental Configuration[34]

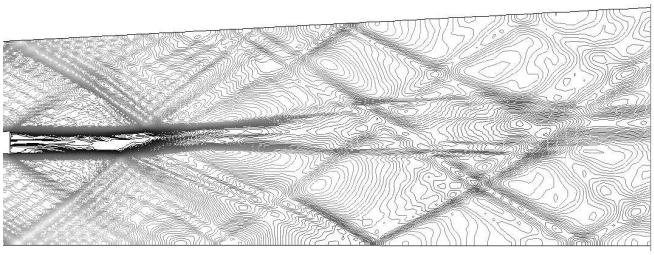

a) Density contours.

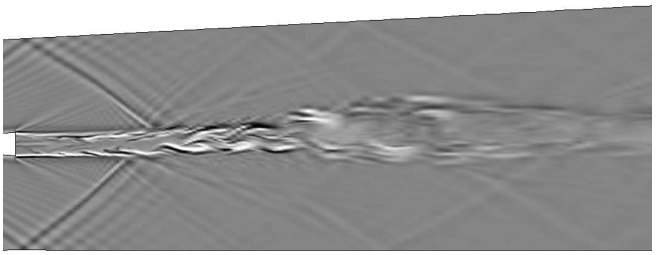

b) $\nabla^2\rho$ field

Fig. 5 Instantaneous density and shadowgraph for the non-reacting case.

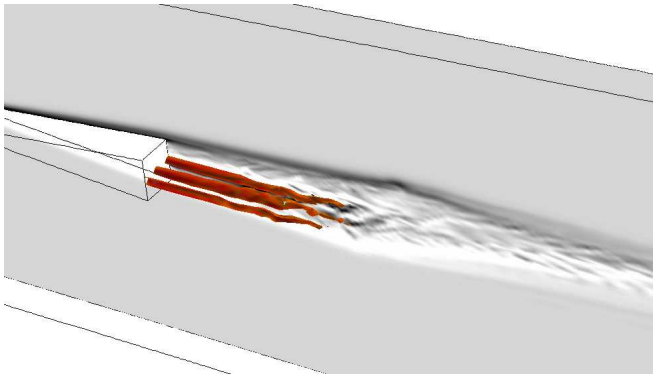

Fig. 3 Hydrogen injection holes / Vorticity for the burning case.

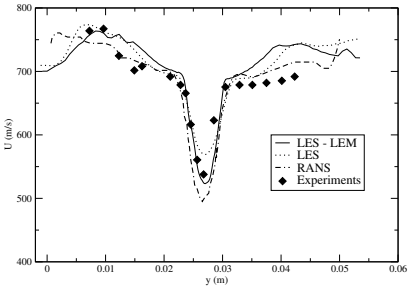

a) x = 58 mm from the base of then wedge

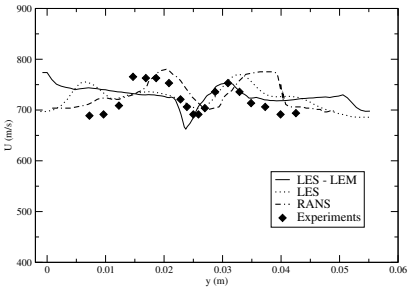

b) x = 90 mm from the base of the wedge

Fig. 6 Mean velocity profile at different stations for non reacting LES.

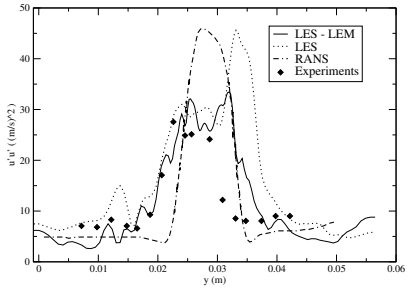

a) x = 115 mm from the base of the wedge

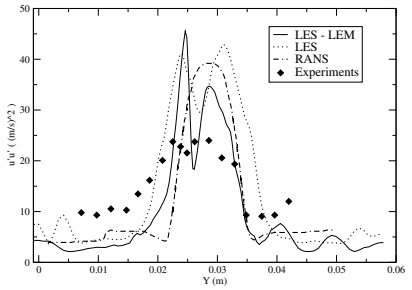

b) x = 140 mm from the base of the wedge

Fig. 7 Axial velocity fluctuation profiles at two different stations for non-reacting LES.

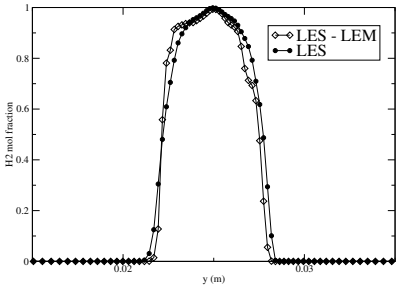

a) x = 58 mm from the base of the wedge

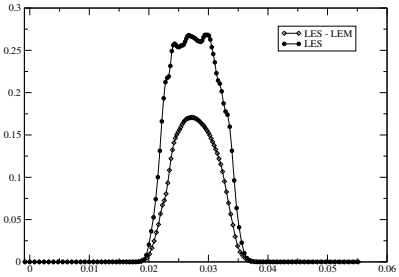

b) x = 90 mm from the base of the wedge

Fig. 8 H_2 **Mol fraction profile at different stations for non-reacting LES.**

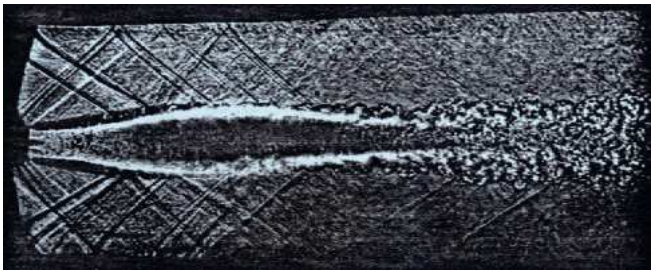

Fig. 9 Shadowgraph of the experimental reacting flow-field

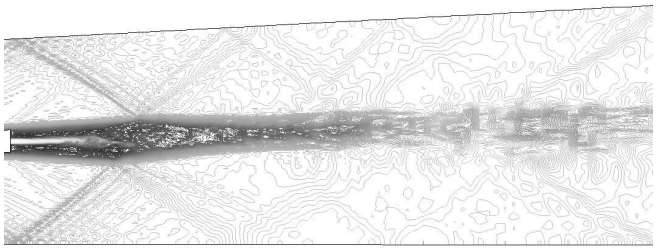

a) Density contours.

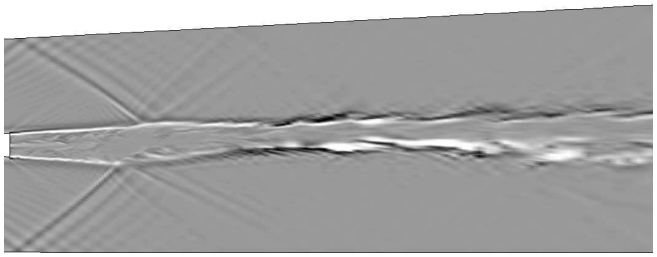

b) $\nabla^2\rho$ field

Fig. 10 Instantaneous density and shadowgraph for the reacting case.

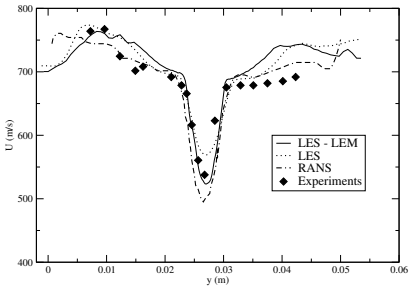

a) x = 58 mm from the base of the wedge

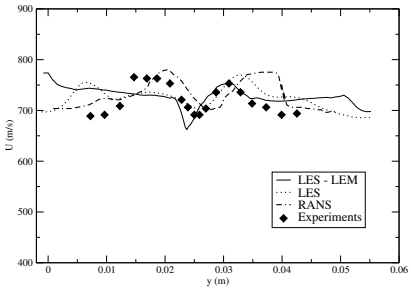

b) x = 140 mm from the base of the wedge

Fig. 11 Mean velocity profiles at different stations for reacting LES.

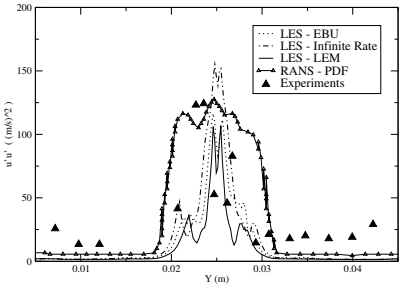

a) x = 11 mm from the base of the wedge

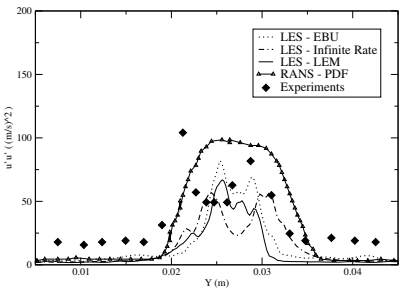

b) x = 58 mm from the base of the wedge

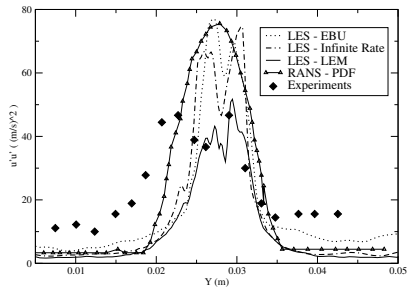

c) x = 90 mm from the base of the wedge

Fig. 12 Axial velocity fluctuation profiles at different stations.

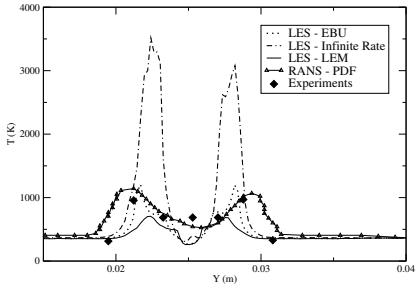

a) x = 11 mm from the base of the wedge

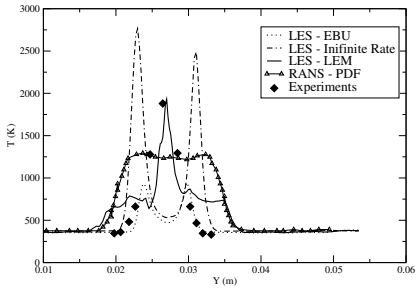

b) x = 58 mm from the base of the wedge

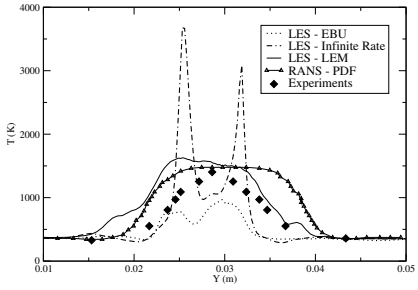

c) x = 156 mm from the base of the wedge

Fig. 13 Temperature profiles at three different stations for the reacting case.